JMEPEG (2018) 27:5656–5664
https://doi.org/10.1007/s11665-018-3670-6

1059-9495/$19.00

Thermal Analysis of Cerium-Treated Chill-Cast Al-23 Si Alloy

V. Vijeesh and K. Narayan Prabhu

(Submitted June 24, 2018; in revised form September 2, 2018; published online October 5, 2018)

The influence of elemental cerium addition on the cooling curve parameters and microstructure of hypereutectic Al-23Si alloy was investigated in this work. The cooling rate of the treated and untreated alloy samples was varied by solidifying the melt against chills of different materials in a stainless-steel tube. The cooling curve was recorded and nucleation temperatures of various phases in the alloy were measured. The results show that the chilling improves the effectiveness of the modifier. The two main phases of the alloy, primary silicon and eutectic silicon, were nucleated at temperatures of about 661.2 and 571.6 °C, respectively. The addition of Ce to slowly cooled alloys resulted in an increase in undercooling temperature of both the phases, with a decrease in its nucleation temperature, whereas the same additions increased the nucleation temperatures in chilled alloys. Based on the thermal analysis results, a relation between thermal analysis parameter (ΔT_G) and silicon particle size of the alloy was proposed.

Keywords Al-23 Si alloy, Ce treatment, cooling rate, modification, refinement, thermal analysis

1. Introduction

CACCA is a technique used to determine various temperature-dependent metallurgical information of the solidifying metal/alloy. Thermo-metallurgical information is obtained by measuring and analyzing the temperature history of the solidifying sample (Ref 1). In the recent past, CACCA was effectively used to predict and quantify various microstructure features like grain size, the level of silicon modification, dendrite coherency point (DCP) and low melting secondary eutectics (Ref 2-5). Further, the technique was also used to find transformation temperatures, latent heat, solid fraction in the melt, phase nucleation temperatures and solidification rates (Ref 6-8).

CACCA involves two stages, (1) continuous measurement and recording of the sample temperature during solidification using a computer interface and (2) identification of the nucleation events of the alloy/metal from the recorded temperature profiles. The obtained solidification curve along with the first derivative curve can be effectively used to detect nucleation temperatures of different microstructure constituent in the alloy (Ref 9). The cooling curve and the time taken for the solidification are greatly influenced by the alloy chemistry. On comparison, the cooling curve of pure metals and eutectic alloys depict a plateau because the entire solidification occurs at a single temperature, whereas hypo- and hypereutectic alloys solidify over a range of temperatures and thus depict a slope in the cooling curve (Ref 10-12).

Owing to superior strength to weight ratio, wear and elevated temperature properties, the aluminum silicon alloys are widely used in automobile industry. The aluminum silicon alloys are broadly classified into hypoeutectic ($<$ 11.6 wt.%), eutectic (11.6-13 wt.%) and hypereutectic (Si $>$ 14 wt.%) alloys (Ref 13). An untreated microstructure of these alloys mainly consists of coarse pro-eutectic aluminum dendrites or primary silicon crystal (hypereutectic) and acicular eutectic silicon dispersed over a eutectic matrix (Ref 14). Mechanical properties, largely dependent on the morphology of the microstructure constituents, are enhanced by melt treatment processes known as 'refinement' and 'modification' (Ref 10, 15). Al-Ti-B master alloys and group II elements like Na and Sr are commonly used to refine and modify aluminum dendrites and eutectic silicon in the hypoeutectic alloys, respectively. On the other hand, primary silicon in the hypereutectic alloy is refined using phosphorus containing master alloys. Apart from chemical additions, chilling and two step heat treatment process also enhances the mechanical properties of the silicon-based aluminum alloys (Ref 10, 16, 17).

The alloy solidification characteristics such as phase nucleation temperature, undercooling and solidification rates change abruptly with modification, refinement and chilling. Hence, an accurate measurement and analysis of the cooling curve parameters would yield the changes brought by melt treatment (refinement/modification) and chilling. Shabestari and Malekan (Ref 2) effectively used CACCA to study the nucleation events in the Al-5Ti-1B grain refined 319 alloy. The liquidus temperature was used as an online prediction tool for grain refinement and casting soundness (Ref 9). Similarly, Chen et al. (Ref 9) found that the temperature difference between the modified and unmodified eutectic silicon (ΔT_e) could be correlated with eutectic silicon modification level. The relation obtained fitted well for modified structure; however, it failed to accommodate the overmodified condition.

Unlike hypoeutectic alloys, the thermal analysis of hypereutectic alloys is rarely carried out. Among very few studies, Robles Hernandez and Sokolowski's (Ref 18) thermal inves-

V. Vijeesh, Department of Mechanical Engineering, N.M.A.M Institute of Technology, Nitte, Udupi 574110, India; and **K. Narayan Prabhu**, Department of Metallurgical and Materials Engineering, National Institute of Technology Karnataka, Srinivasnagar, Surathkal, Mangaluru 575025, India. Contact e-mail: prabhukn_2002@yahoo.co.in.

tigation of hypereutectic alloys (390.1 and 393.2) produced firm results on solidification behavior of primary silicon in hypereutectic alloys. According to them, Si atoms agglomerate at higher temperatures to form primary silicon. Hence, the size and shape of the primary silicon depend on the silicon agglomerates formed at higher temperatures. However, the effect of refinement or chemical addition on the solidification behavior of hypereutectic alloys is yet to be investigated. Like hypoeutectic alloys, the cooling curve and microstructure of hypereutectic alloy is also influenced by the chemical composition. The morphology of primary silicon crystals is altered by the addition of phosphorus. Although, phosphorous effectively refines the primary silicon, its inefficiency in modifying the eutectic silicon is well known (Ref 19). Alternatively, the present authors have reported the ability of Ce in improving the mechanical property of the Al-23Si alloy by concurrent refinement of primary crystal and eutectic in unchilled alloys (Ref 20).

The present study investigates the effect of varying addition of cerium on the primary and eutectic nucleation temperatures. The CACCA technique was used to measure and determine various phases in the solidifying sample. In addition, an attempt is made to correlate microstructural features with the cooling curve parameters considering the effects of cooling rate, refinement and modification.

2. Materials and Methods

The chemical composition of the hypereutectic alloy used for the investigation is given in Table 1. Alloy samples (350 g) cut form large ingot were heated to a temperature of about 850 °C using a resistance coil electric furnace in a clay-graphite crucible. The melted alloy was then added with different concentrations of Ce (0.5, 1.0, 1.5, 2.0 wt.%) at about thirty minutes prior to pouring. The required quantity of Ce, cut from a 99% Ce ingot (Alfa Aesar), was dipped in the melt using a stainless-steel tong until it was melted. The melt temperature was carefully monitored and controlled during the process to avoid any overheating and oxidation of the melt. After thirty minutes, the melted alloy was top poured to a stainless-steel (type 304) tube with metal chill at the bottom to promote directional solidification. The dimensions of the SS tube and chills are shown in Fig. 1. For slow solidification, the tube was placed on the sand. Chills of varying thermal conductivities (copper-385 W/m-K, brass-125 W/m-K and stainless steel-17 W/m-K) were used to alter the heat absorption and cooling rates. The heat loss from SS tube and chill surface was minimized by covering it with thermal insulation material (glass–wool). A K-type thermocouple was used to measure the temperature of the cooling sample, which in turn was recorded using a high-speed data acquisition system (National Instruments) interfaced with computer.

For metallographic analysis, the samples sectioned from castings were fine polished using metallographic grit papers and 0.3 μm de-agglomerated alumina solution in a rotating disk polisher. The microstructures of the untreated and treated samples were captured using a scanning electron microscope (JEOL JSM-6380LA). Primary silicon and eutectic particle characteristics such as length, area, width and perimeter were measured using an auxiliary image analysis software (Axio Vision). The characteristics each particle were measured from the microstructures obtained various locations in the sample. The procedure was repeated for samples of all trials of treated as well as untreated alloys. The recorded values of each sample were then used to find out the mean size and standard deviation. The roundness factor was calculated using measured perimeter and area value of each particle as $P^2/4\pi A$.

3. Results and Discussion

Cooling curve of the untreated alloy sample solidified against sand (without any chill) is shown in Fig. 2. The characteristic points of various nucleation events corresponding to the deflections in first derivate curve (FDC) are marked in Fig. 2. The description of the thermal analysis parameters is shown in Table 2. The solidification curve of the binary hypereutectic Al-Si alloy accounts for nucleation events of pro-eutectic primary silicon and eutectic phase, respectively. T_N (No. 1 in Fig. 2) corresponds to the point where the nucleation of the primary silicon starts and is identified by a deflection in the derivative curve. T_{min} (No. 2) is a temperature in the cooling curve corresponding to the point where derivative curve

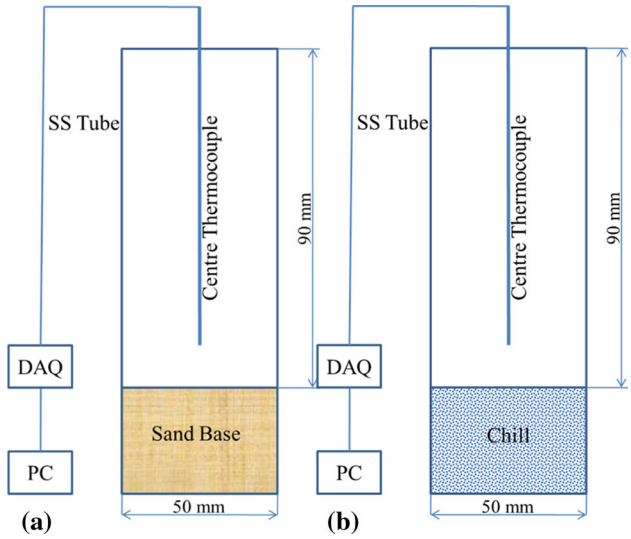

Fig. 1 Schematic sketch of solidification setup (a) without chill and (b) with chill

Table 1 Composition of the alloy used for experiments

Elements	Si	Cu	Fe	Mg	Mn	Ni	Al
(wt.%)	23 ± 1	0.4 ± 0.1	1.1 ± 0.1	0.03 ± 0.01	0.05 ± 0.01	0.003	Rest

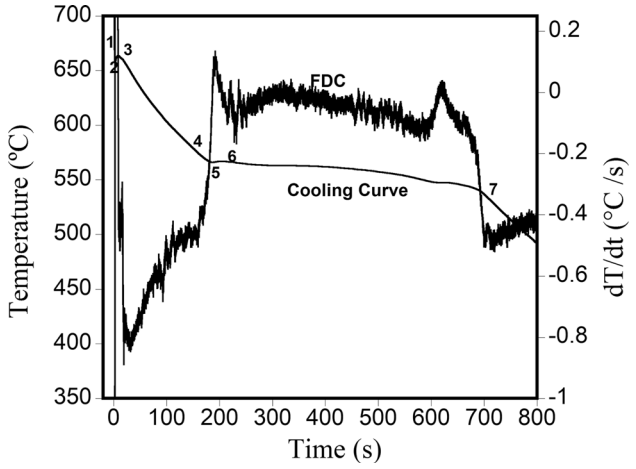

Fig. 2 Cooling and first derivative curves of untreated and unchilled Al-23 Si alloy

Table 2 Thermal analysis parameters

1	T_N (Si)	Primary silicon nucleation temperature
2	T_{min} (Si)	Primary silicon minimum nucleation temperature
3	T_G (Si)	Primary silicon growth temperature
4	T_N (Eut)	Eutectic nucleation temperature
5	T_{min} (Eut)	Eutectic minimum nucleation temperature
6	T_G (Eut)	Eutectic growth temperature
7	T_S	Solidus temperature

reaches zero. T_G (No. 3) is the temperature at which the particles start growing. The numbers 4, 5 and 6 correspond to the characteristic points of eutectic nucleation, and T_s (7) is a point at which solidification completes. Other thermal analysis parameters related to nucleation, such as T_N, T_{min}, T_G, ΔT_G (growth temperature difference) and the degree of undercooling ($T_{under} = T_N - T_{min}$), were calculated from the above 7 points. Further, the thermal parameters were analyzed and compared to evaluate the influence of various concentrations of cerium.

Figure 3 shows the cooling curve of the Ce-treated alloy samples for different chilling rates. The corresponding nucleation temperature characteristics of each alloy sample are tabulated in Table 3. As observed in Fig. 3, the cooling curves are significantly influenced by the chilling and Ce melt treatment. In the unchilled (cooling rate 0.2 °C/s) and untreated condition, the alloy nucleation started at 661.2 °C and ended at 530 °C. Further, the nucleation of primary silicon and alloy solidus temperatures decreased with Ce addition to unchilled alloys, whereas the same increased with chilling. The time for solidification decreased with increasing cerium concentrations, for both chilled and unchilled conditions. However, alloys with 2 wt.% Ce showed an opposing trend with chilling as the nucleation temperatures showed a decreasing trend compared to alloys treated with 1.5 wt.% Ce.

In addition, Fig. 4 shows the variation of primary silicon nucleation temperature with respect to Ce concentration and chilling. Under lower cooling conditions (without chill), the primary silicon in an untreated alloy nucleated at temperature of about 661.2 °C with an undercooling of 3.5 °C. But, a decrease in primary silicon nucleation temperature was observed with an increase in cooling rate (chilling); however, the undercooling increased with addition. According to Robles Hernandez and Sokolowski (Ref 18), the primary silicon nucleates from the Si clusters formed at higher temperatures. At lower cooling rates, these silicon clusters arrange themselves into a tetrahedron cluster and agglomerate into fivefold twinning polyhedral which would act as a stable nucleant for primary silicon. These low-energy nucleants favor the faceted growth of fivefold silicon crystals (Ref (Ref 20). But, higher solidification rates would suppress the agglomeration of such Si clusters and subsequently hinder the formation of former stable epitaxial nucleation sites. Consequently, the primary silicon will be forced to nucleate on high-energy sites as fine Si clusters from highly undercooled melts.

The chilling enhances the effectiveness of cerium on nucleation temperatures. An increase in primary silicon nucleation temperature was observed with an increase in cerium and chilling rate. Although, a decreasing trend in primary silicon nucleation temperature was observed beyond 1.5 wt.%. This would be due to the formation of primary silicon from τ_2 phase (Ref 20). Based on Al-Ce-Si phase diagram (Ref 20), at lower concentrations of Ce, the aluminum, silicon and cerium combine to form a metastable τ_1 phase, which would dissociate to form finer primary silicon at higher temperatures. On the other hand, higher concentrations of Ce (>1.5 wt.%) would result in the formation of τ_2 phase, which do not favor the formation of primary silicon, and hence, the temperature decreases thereafter.

An increase in undercooling temperature of untreated alloy with cooling rate shown in Fig. 4 indicates the degree of difficulty involved with nucleation of primary silicon. Hence, it can be inferred that at equilibrium solidification rates, the Si atom clusters lower the energy by spontaneously forming into fivefold heterogeneous nucleation agents (Ref 20) and the nucleation of primary silicon occurs more easily from these sites from less undercooled melt. On the other hand, the agglomeration of such low-energy Si clusters does not happen in chilled alloys because of very high heat absorption rate, which would restrict the formation of fivefold nucleation sites and the nucleation of primary silicon. As a result, the undercooling increases and primary silicon is forced to nucleate from non-favorable nucleation sites.

Unlike eutectic silicon in hypo eutectic alloys, the eutectic silicon in hypereutectic alloys are nucleated on the primary silicon. Hence, the energy barrier for the nucleation of eutectic is dependent on the primary silicon morphology. The eutectic silicon nucleation temperatures for various additions of Ce and chilling are given in Table 3. Figure 5(a) shows the variation in eutectic silicon nucleation temperatures with Ce addition. The undercooling temperature associated with the eutectic nucleation is shown in Fig. 5(b). The eutectic phase temperature, about 571.6 °C, of untreated alloy, decreased with an increase in chilling rate along with an increase in undercooling temperature. The cerium melt treatment had more effect on the T_{min} temperature than on the T_N. The observed decrease in undercooling temperature with cerium and chilling indicates that higher cooling rates favor the nucleation of eutectic silicon, as the eutectic silicon in chilled alloys were nucleated at much higher temperature than unchilled alloys.

Wu et al. (Ref 21) reported that the eutectic silicon in hypereutectic alloys nucleates on the primary silicon. The nucleation frequency of eutectic silicon in P-treated alloy was

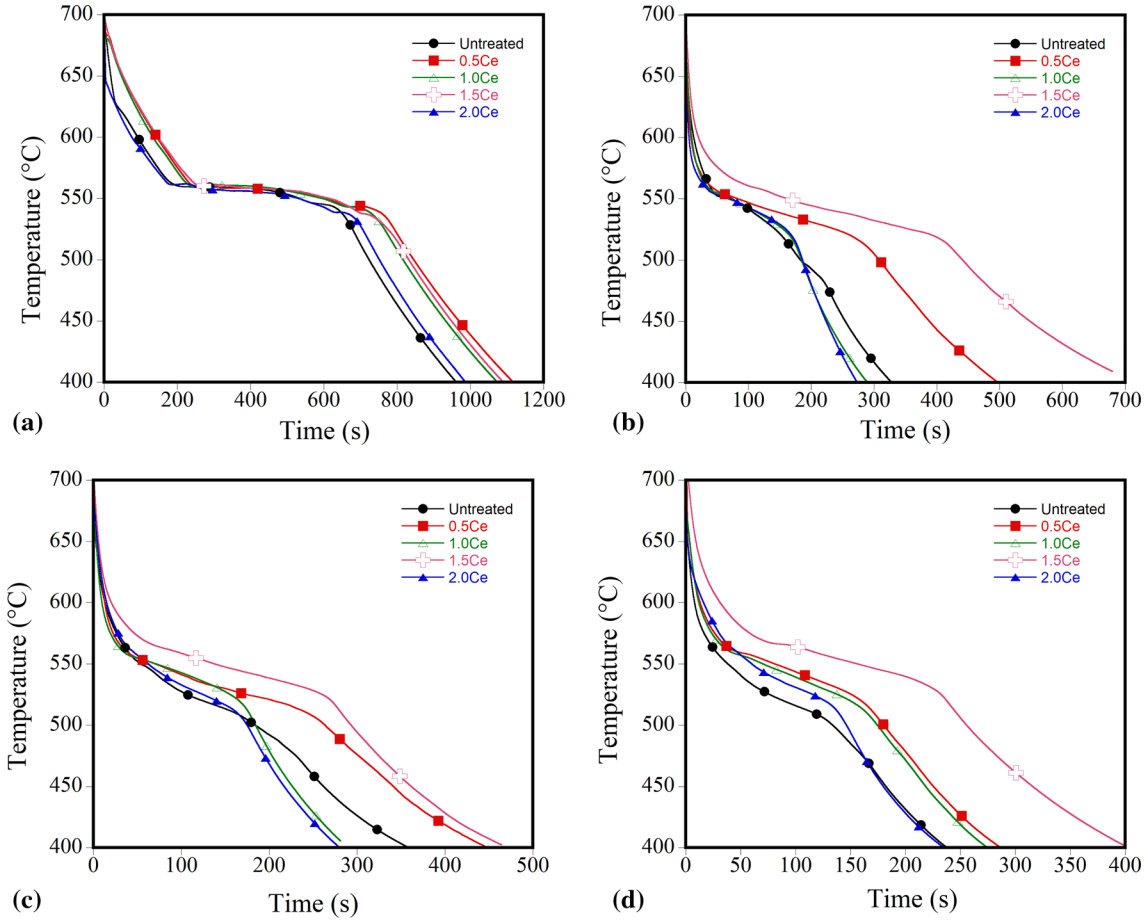

Fig. 3 Cooling curves of Al-23%Si alloys with varying Ce content solidified on (a) unchilled, (b) stainless steel, (c) brass, (d) copper chills

Table 3 Cooling curve analysis of Ce added Al-23% Si alloys

		Primary silicon				Eutectic silicon				
	Ce wt.%	$T_N(\alpha)$, °C	$T_{min}(\alpha)$, °C	$T_G(\alpha)$, °C	$\Delta T_N(\alpha)$, °C	T_N(Eut), °C	T_{min}(Eut), °C	T_G(Eut), °C	ΔT_N(Eut), °C	T_S, °C
Unchilled	Untreated	661.2	657.7	663.7	3.5	571.6	566.1	566.9	5.5	530
	0.5Ce	653.7	647.8	648.7	5.9	574	560.2	560.5	13.8	520
	1Ce	651.3	645.6	646.9	5.7	573.8	559.7	560.9	14.1	513
	1.5Ce	642.6	641.9	642.5	0.7	571.3	559.9	560.8	11.4	506
	2Ce	640.5	640	641.2	0.5	573.9	562.5	562.6	11.4	503
Copper	Untreated	656	647.8	647	8.2	566	558	557.9	3	520
	0.5Ce	671	669.1	664.7	1.9	570.8	568.3	565.9	2.5	508
	1Ce	687.2	685.5	680	1.7	576	572.1	571.4	3.9	510
	1.5Ce	729.5	727.8	725	1.7	578	575.1	574.8	2.9	512
	2Ce	698.9	697	696.5	1.9	574.7	572.1	578.6	2.6	513
Brass	Untreated	658.3	654	654	4.3	566	559	558.2	3.5	522
	0.5Ce	675	674.7	674	0.3	562.3	561.9	561.3	0.4	523
	1Ce	684.7	684.4	683.5	0.3	565.7	565.3	564.1	0.4	525
	1.5Ce	730.5	730.2	729.5	0.3	573.1	572.1	571.4	1	527
	2Ce	681.8	679	678.5	2.8	573.5	571.2	571	2.3	526
Stainless steel	Untreated	659.7	656	657.3	3.7	566	562	550.3	4	525
	0.5Ce	660	658	657	2	566.8	564.2	564	2.6	526
	1Ce	665.7	664	663.5	1.7	570.5	567.5	568.5	3	527
	1.5Ce	730	728	727.7	2	571.2	569.1	568.5	2.1	529
	2Ce	680	675	674	5	570.2	567.3	567.1	2.9	527

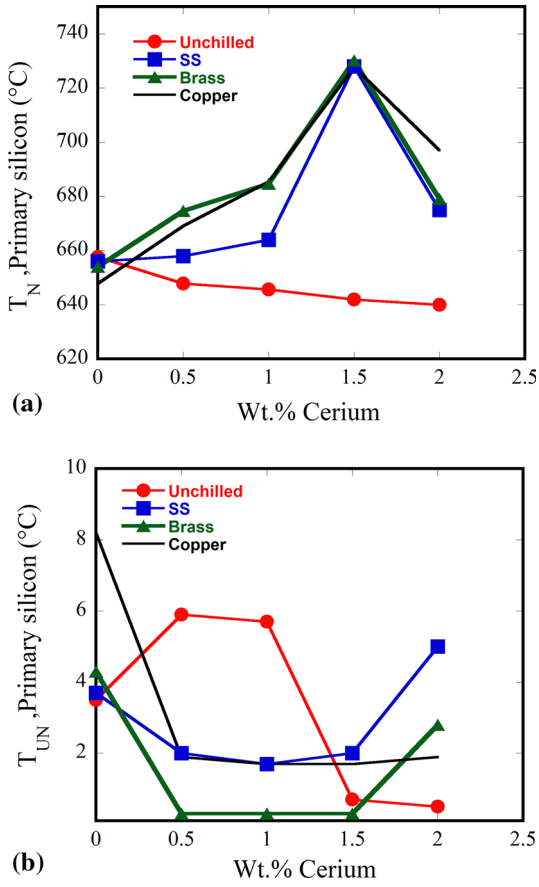

Fig. 4 Effect of Ce additions and cooling rates on the primary silicon (a) nucleation temperature and (b) degree of undercooling

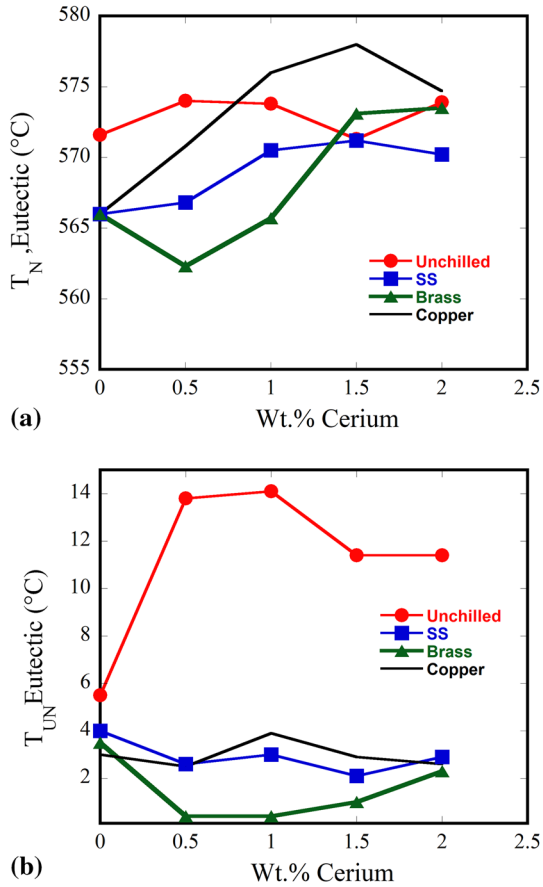

Fig. 5 Effect of Ce additions and cooling rates on the eutectic silicon (a) nucleation temperature and (b) degree of undercooling

higher than the untreated alloy, and it was supposedly due to the refined polyhedral primary silicon, which acted as an ideal heterogenous site for the nucleation of eutectic silicon. The same mechanism can be correlated with the findings of the present study as well. The cerium addition and chilling led to the nucleation of finer primary silicon, which favored easy nucleation of eutectic silicon from less undercooled melt. However, the theory does not hold good for slowly cooled Ce-treated alloys. At lower cooling rates, the cerium present in the melt does not allow the eutectic silicon to nucleate and grow from the primary silicon. The decrease in the eutectic nucleation temperature along with an increase in undercooling temperature is an evidence for the non-heterogenous nucleation; however, the added cerium at that cooling rate resulted in silicon modification. On the other hand, decreasing undercooling in chilled alloys indicates that Ce favored the heterogeneous nucleation of eutectic silicon, preferably from refined polyhedral primary silicon. Hence, the eutectic Si nucleated from the refined primary silicon at higher temperatures and less undercooled melt would grow easily as acicular silicon.

Figure 6 shows the SEM micrographs of Ce-treated Al-23Si hypereutectic alloys solidified against various metallic chills. As seen in Fig. 6(a), when untreated, the lower cooling rates led to the formation of large star-shaped primary silicon crystals and coarse needle-shaped eutectic silicon (acicular). According to Pei and Hosson (Ref 22, 23), such large primary silicon with star-like shapes are grown from single decahedral nucleus consisting of five branches of silicon tetrahedrons sharing common axis. Further growth of each branch can be explained by Twin Plane Re-entrant Edge (TPRE) growth mechanism, as the silicon particles grow by maintaining a 141° groove at branch tips. Besides, the growth of primary silicon also depends on the melt undercooling and solidification rate. The observed star-like morphologies of primary silicon are reported to be formed in largely undercooled melts (Ref 24).

The Ce additions had transformed the coarse star-shaped silicon crystals into fine polyhedral-shaped crystals. The refinement was more effective with chilling due to the synergistic action of cerium melt treatment and chilling rate as shown in Fig. 7(a). A decrease in silicon particle size was observed with an increase in cerium concentrations for both unchilled and chilled conditions. Comparison between CACCA and microstructure results reveals that the lower degree of undercooling favors the formation of finer polyhedral primary silicon; however, it contradicts the findings of Ref 24. According to their thermal analysis results, the transformation of primary silicon from star-shaped crystals to polyhedral crystals occurs at larger undercooling. Certainly, they did not consider the nucleation of primary silicon from heterogeneous nucleation sites with lesser undercooling. In the present alloy, the Ce additions yielded polyhedral primary silicon from the less undercooled melt. During P refinement, the P will combine with Al to form AlP compounds in the melt, a favorable heterogenous nucleation site for silicon (Ref 25); however, there is no reported literature on Ce nucleating the silicon.

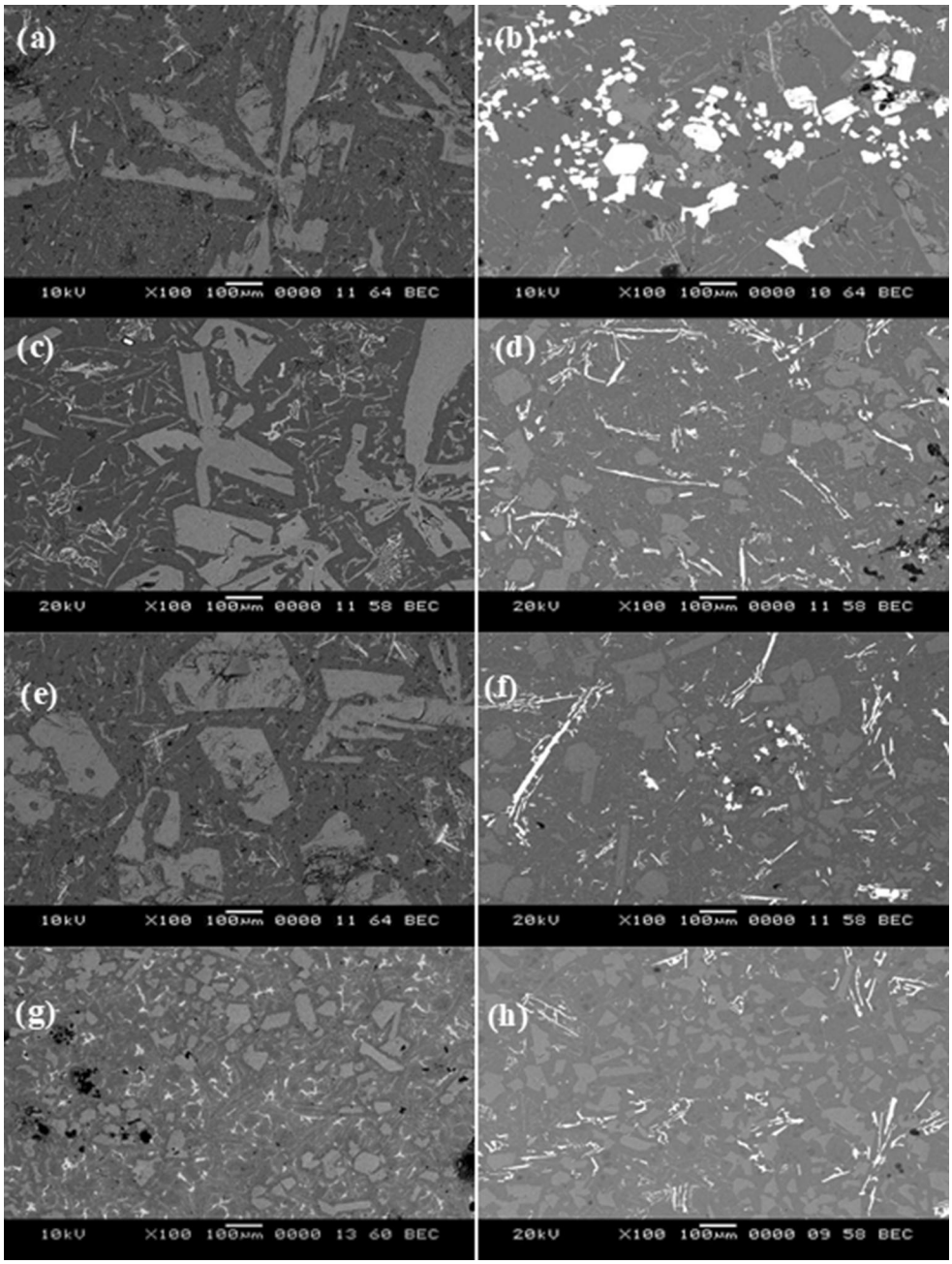

Fig. 6 Micrographs of untreated and 1.5% Ce-treated alloys (a) untreated–without chill, (b) treated–without chill, (c) untreated–stainless-steel chill, (d) treated–stainless-steel chill, (e) untreated–brass chill, (f) treated–brass chill, (g) untreated–copper chill (g) Ce-treated–copper chill

Although the cerium hardly modified the eutectic silicon in chilled alloys, it certainly refined the eutectic Si in slowly cooled alloys. The particle characteristics (length, width, perimeter) of the eutectic silicon formed in the alloys solidified under various chilling conditions are shown in Table 4. Subsequently, Fig. 7(b) shows the variation in eutectic particle length with cerium additions. Although the influence of cerium varied with cooling rate, in unchilled alloys, the eutectic silicon size decreased with an increase in cerium concentration owing to the modification effect. A decrease in roundness factor with cerium treatment is an evidence for the modification of eutectic silicon particle. However, at higher chilling rates, the cerium in the melt favored the growth of eutectic silicon. The microstructure analysis is in complete agreement with the CACCA analysis results, since the decrease in the undercooling temperature and reduction in eutectic particle size with Ce treatment is a proof for the above-mentioned theory, for the nucleation of eutectic silicon from the refined primary silicon (Ref 21). Under favorable conditions, the eutectic silicon easily nucleates on primary silicon from less undercooled melt and grows acicular in nature. In this connection, the decrease in undercooling with addition of Ce indicates the ease with which eutectic silicon was nucleated from primary silicon.

Since Ce treatment had significant influence on the primary silicon nucleation temperature and primary silicon size, the results could be used to obtain a relation to predict the microstructure features of the alloy. The obtained results account for all the possible behaviors and variations of the

primary silicon size with cooling rate and nucleation temperatures. Hence, a dimensionless parameter, in terms of equivalent diameter of the primary silicon, was proposed. Figure 8 shows the correlation obtained between the thermal analysis growth parameter (ΔT_G) and the dimensionless parameter (primary silicon characteristic). The primary silicon characteristic parameter is defined as the ratio of equivalent diameter of refined primary silicon particle to the equivalent diameter of unrefined primary silicon particle. This characteristic parameter could be used to quantify the primary silicon refinement in Al-Si alloys. Lower the value of ΔT_G, higher the refinement (smaller primary silicon) and vice versa.

Similarly, Fig. 9 shows the relation between eutectic growth temperature parameter (ΔT_G) and cooling rate for various concentrations of cerium. Unlike primary silicon, the dimensionless parameter did not show any relation with eutectic roundness factor in Al-23Si alloy, as Ce in combination with chilling, favored eutectic growth than modification. However,

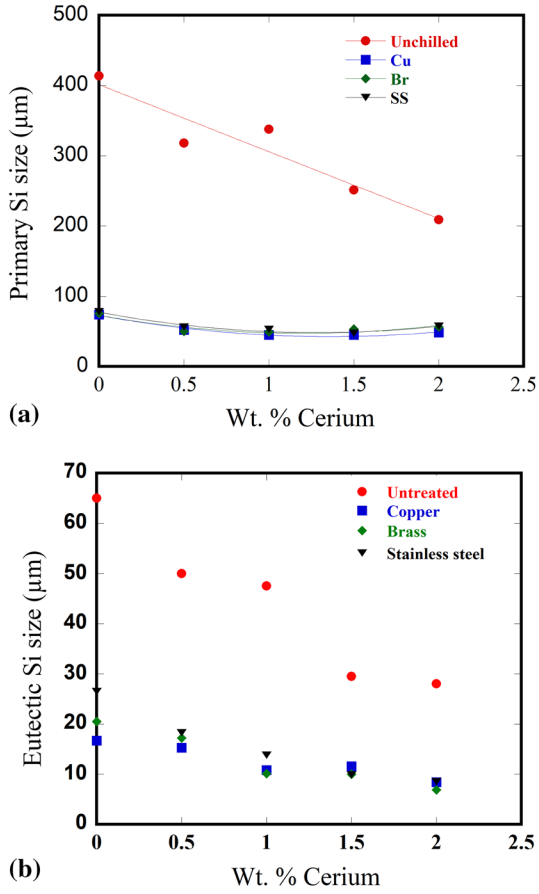

Fig. 7 Synergistic effect of cerium and cooling rate on (a) primary silicon size and (b) eutectic silicon size

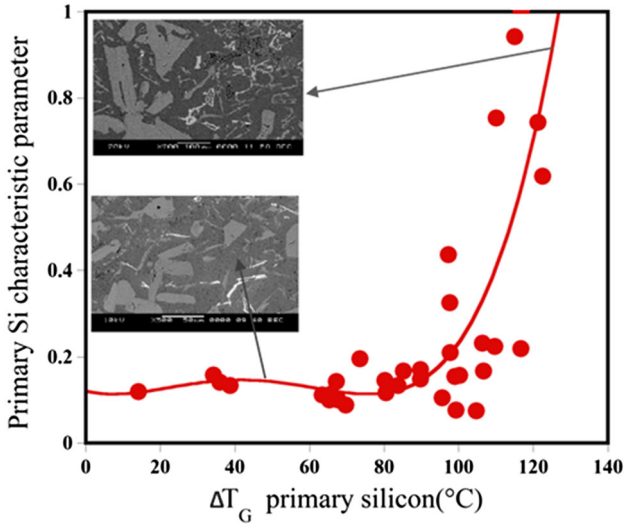

Fig. 8 Correlation between thermal analysis parameter, ΔT_G, and the primary silicon characteristic parameter in Al-23 Si alloy

Table 4 Effect of cerium on eutectic silicon characteristics

	wt.% Ce	Length, µm	Aspect ratio	Area, µm^2	Perimeter, µm	Roundness factor
Unchilled	0	80 ± 30	13.3 ± 2	250 ± 50	150 ± 30	7.16
	0.5	70 ± 10	10.0 ± 1	220 ± 20	130 ± 10	6.11
	1	65 ± 5	8.1 ± 1	200 ± 20	124 ± 5	6.12
	1.5	65 ± 5	7.2 ± 1	190 ± 10	120 ± 4	6.03
	2	68 ± 8	7.6 ± 1	198 ± 10	123 ± 5	6.08
Stainless steel	0	40 ± 15	8.0 ± 1.8	120 ± 20	90 ± 15	5.37
	0.5	38 ± 10	6.3 ± 0.6	115 ± 10	90 ± 8	5.60
	1	35 ± 5	6.4 ± 0.5	110 ± 8	88 ± 5	5.60
	1.5	30 ± 5	6.3 ± 0.4	110 ± 10	90 ± 4	5.86
	2	30 ± 5	6.7 ± 0.2	108 ± 12	92 ± 3	6.23
Brass	0	20 ± 10	6.7 ± 1.5	50 ± 10	50 ± 10	3.98
	0.5	19 ± 5	6.6 ± 0.6	45 ± 5	52 ± 5	4.78
	1	18 ± 4	6.4 ± 0.4	40 ± 6	50 ± 2	4.97
	1.5	18 ± 4	6.4 ± 0.5	38 ± 4	50 ± 3	5.23
	2	19 ± 3	6.6 ± 0.5	36 ± 2	49 ± 2	5.31
Copper	0	16 ± 5	5.3 ± 1	20 ± 5	30 ± 8	3.58
	0.5	14 ± 3	6.4 ± 0.8	18 ± 2	30 ± 2	3.98
	1	14 ± 2	6.7 ± 0.8	16 ± 1	30 ± 1	4.47
	1.5	12 ± 3	6.7 ± 1.5	15 ± 0.5	30 ± 1	4.77
	2	12 ± 3	7.1 ± 0.4	15 ± 1	30 ± 1.5	4.77

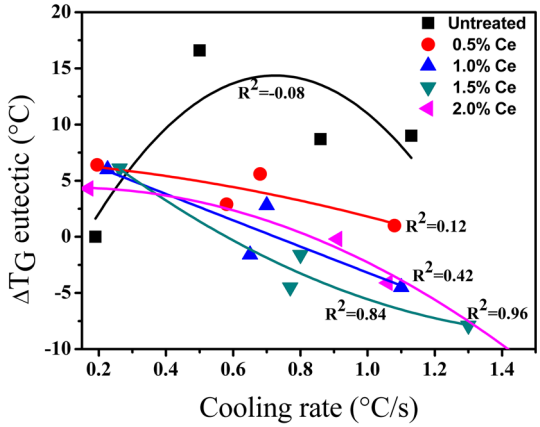

Fig. 9 Eutectic growth temperature differences vs. cooling rate for varying content of Ce

eutectic growth temperature qualitatively indicates the modification level in the alloy. The decrease in ΔT_G value with chilling and cerium addition indicates that the formation of large acicular eutectic silicon, due to the refinement of primary silicon. On the other hand, the lower undercooling values suggest that the nucleation of eutectic silicon occurs easily at lower ΔT_G; however, an increase in ΔT_G values in unchilled alloys suggests that the silicon modification occurred due to the addition of cerium.

4. Conclusions

Based on CACCA and metallographic analysis of cerium-treated hypereutectic Al-23Si alloy, the following conclusions were drawn.

1. The primary and eutectic phases in untreated unchilled alloy nucleated at temperatures of about 661.2 and 571.6 °C with an undercooling of 3.5 and 5.5 °C, respectively.
2. The effectiveness of cerium melt treatment on the primary and eutectic nucleation temperatures varied with chilling rate. In unchilled conditions, the Ce suppressed the nucleation temperatures by increasing the undercooling required for nucleation.
3. Under chilling, the presence of Ce favored the nucleation of primary and eutectic silicon by nucleating it at higher temperatures from the less undercooled melt.
4. The effect of Ce was more significant at chilled conditions than in unchilled conditions, as it refined primary silicon. However, the eutectic silicon modification was observed only at lower cooling rates.
5. A good fit was obtained between ΔT_G and the primary silicon particle size parameter. The extent of refinement of silicon could be assessed using this parameter.

Acknowledgments

One of the authors (VV) gratefully acknowledges the faculties and laboratory technicians of the Department of Metallurgical and Materials Engineering, NITK Surathkal, India, for their support and assistance in completing this work as a part of the Ph.D. thesis.

References

1. A. Niklas, U. Abaunza, A.I. Fernandez-Calvo, J. Lacaze, and R. Suarez, Thermal Analysis as a Microstructure Prediction Tool for A356 Aluminium Parts Solidified Under Various Cooling Conditions, *China Foundry*, 2011, **8**(1), p 89–95
2. S.G. Shabestari and M. Malekan, Assessment of the Effect of Grain Refinement on the Solidification Characteristics of 319 Aluminium Alloy Using Thermal Analysis, *J. Alloys Compd.*, 2010, **492**, p 134–142
3. X. Chen, H. Geng, and Y. Li, Study on the Eutectic Modification Level of Al-7Si Alloy by Computer Aided Recognition of Thermal Analysis Cooling Curves, *Mater. Sci. Eng. A*, 2006, **419**, p 283–289
4. M.B. Djurdjevic, J.H. Sokolowski, and Z. Odanovic, Determination of Dendrite Coherency Point Characteristics Using First Derivative Curve Versus Temperature, *J. Therm. Anal. Calorim.*, 2012, **109**, p 875–882
5. S.G. Shabestari and S. Ghodrat, Assessment of Modification and Formation of Intermetallic Compounds in Aluminium Alloy Using Thermal Analysis, *Mater. Sci. Eng. A*, 2007, **467**, p 150–158
6. V. Vijeesh and K.N. Prabhu, Assessment of Latent Heat and Solid Fraction of Al-22Si Alloy Using Newtonian and Fourier Analysis Techniques, *Mater. Sci. Forum*, 2015, **830–831**, p 321–324
7. V. Vijeesh and K.N. Prabhu, The Effect of the Addition of Ce and Sr on the Solidification Path of Al-8Si-2Cu Alloy, *Trans. Indian Inst. Met.*, 2015, **68**(6), p 1119–1123
8. S.G. Shabestari and M. Malekan, Thermal Analysis Study of the Effect of the Cooling Rate on the Microstructure and Solidification Parameters of 319 Aluminium Alloy, *Can. Metall. Q.*, 2005, **44**, p 305–312
9. M. Djurdjevic, H. Jiang, and J. Sokolowski, On-Line Prediction of Aluminium–Silicon Eutectic Modification Level Using Thermal Analysis, *Mater. Charact.*, 2001, **46**, p 31–38
10. R. Aparicio, G. Barrera, G. Trapaga, M. Ramirez-Argaez, and C. Gonzalez-Rivera, Solidification Kinetics of a Near Eutectic Al-Si Alloy, Unmodified and Modified with Sr, *Met. Mater. Int.*, 2013, **19**, p 707–715
11. Ishan-ul-haq, J. Shin, and Z. Lee, Computer-Aided Cooling Curve Analysis of 356 Aluminum Alloy, *Met. Mater. Inter.*, 2004, **10**(1), p 89–96
12. M. Faraji, I. Todd, and H. Jones, Effect of Phosphorus and Strontium Additions on Formation Temperature and Nucleation Density of Primary Silicon in Al-19 wt pct Si Alloy and Their Effect on Eutectic Temperature, *Metall. Mater. Trans. A*, 2009, **40**, p 1710–1715
13. G. Sigworth, Fundamentals of Solidification in Aluminum Castings, *Int. J. Met. Cast.*, 2014, **8**(1), p 7–21
14. L. Backerud, G. Chai, and J. Tamminen, Solidification Characteristics of Aluminum Alloys, Foundry Alloys, *Foundry Alloys AFS Des Plaines IL*, 1990, **2**, p 71–229
15. J.G. Li, B.Q. Zhang, L. Wang, W.Y. Yang, and H.T. Ma, Combined Effect and Its Mechanism of Al-3wt.% Ti-4wt.% B and Al-10wt.% Sr Master Alloy on Microstructures of Al-Si-Cu Alloy, *Mater. Sci. Eng. A*, 2002, **328**, p 169–176
16. K. He, F. Yu, D. Zhao, and L. Zuo, Effect of Phosphorus Modification on the Microstructure and Mechanical Properties of DC Cast Al-17.5Si-4.5Cu-1Zn-0.7 Mg-0.5Ni Alloy, *Trans. Indian Inst. Met.*, 2010, **62**, p 367–371
17. E. Sjolander and S. Seifeddine, The Heat Treatment of Al-Si-Cu-Mg Casting Alloys, *J. Mater. Process. Technol.*, 2010, **210**, p 1249–1259
18. F.C. Robles Hernández and J.H. Sokolowski, Thermal Analysis and Microscopical Characterization of Al-Si Hypereutectic Alloys, *J. Alloys Compd.*, 2006, **419**, p 180–190
19. M. Zuo, X. Liu, H. Dai, and X. Liu, Al-Si-P Master Alloy and Its Modification and Refinement Performance on Al-Si Alloys, *Rare Met.*, 2009, **28**, p 412–417
20. V. Vijeesh and K.N. Prabhu, The Effect of Chilling and Ce Addition on the Microstructure and Mechanical Properties of Al-23Si Alloy, *J. Mater. Eng. Perform.*, 2017, **26**, p 343–349

21. Y. Wu, X. Liu, B. Jiang, and C. Huang, Eutectic Nucleation in Al-25wt.%Si Alloy Through DSC, *Rare Met.*, 2010, **29**, p 62–65
22. Y.T. Pei and JThM De Hosson, Five-Fold Branched Si Particles in Laser Clad Al-Si Functionally Graded Materials, *Acta Mater.*, 2001, **49**, p 561–571
23. Y.T. Pei and JThM De Hosson, Materials Produced by Laser Cladding, *Acta Mater.*, 2000, **48**, p 2617–2624
24. H.S. Kang, W.Y. Yoon, K.H. Kim, M.H. Kim, and Y.P. Yoon, Microstructure Selections in the Undercooled Hypereutectic Al-Si Alloys, *Mater. Sci. Eng. A*, 2005, **404**, p 117–123
25. Z. Ying, Y. Dan-Qing, L. Wang-Xing, R. Zhi-Sen, Z. Qun, and Z. Jun-Hong, Transformation of Microstructure After Modification of A390 Alloy, *Trans. Nonferrous Met. Soc. China*, 2007, **17**, p 413–417